Plasma Walls Beyond the Perfect Absorber Approximation for Electrons

Franz X. Bronold, Rafael L. Heinisch, Johannes Marbach, and Holger Fehske

***Abstract*—Plasma walls accumulate electrons more efficiently than ions, leading to wall potentials which are negative with respect to the plasma potential. Theoretically, walls are usually treated as perfect absorber for electrons and ions, implying perfect sticking of the particles to the wall and infinitely long desorption times for particles stuck to the wall. For electrons, we question the perfect absorber model and calculate, specifically for a planar dielectric wall, the electron sticking coefficient s_e and the electron desorption time τ_e. For the uncharged wall, we find $s_e \ll 1$ and $\tau_e \approx 10^{-4}$ s. Thus, in the early stage of the build-up of the wall potential, when the wall is essentially uncharged, the wall is not a perfect absorber for electrons. For the charged wall, we find $\tau_e^{-1} \approx 0$. Thus, τ_e approaches the perfect absorber value. But s_e is still only of the order of 10^{-1}. Calculating s_e as a function of the wall potential and combining this expression with the quasi-stationary balance equations for the electron and ion surface densities, we find the self-consistent wall potential, including surface effects, to be 30% of the perfect absorber value.**

***Index Terms*—Plasma sheath, plasma–wall interaction, wall charging.**

I. Introduction

MACROSCOPIC objects in contact with an ionized gas—plasma walls—act as sinks and sources for the charged and uncharged particles of the plasma. Because electrons are collected more efficiently than ions, walls are negatively charged and thus shielded from the bulk plasma by a space-charge depletion layer (plasma sheath). But not only the spatial homogeneity of the plasma is strongly affected by the wall. Surface-supported electron–ion recombination and secondary electron emission severely modify the overall charge balance of the discharge. Particularly in dusty plasmas [1]–[3] and solid-state-based microdischarges [4], [5] the wall becomes an integral part of the plasma.

The microscopic understanding of the build-up of the negative wall potential is in a rather rudimentary stage. It is usually based on the assumption that electrons and ions hitting the wall are instantaneously annihilated which is the same as to say the wall is a perfect absorber for electrons and ions. The wall potential arising from this picture is the one which equalizes at the wall the electron and ion influxes from the plasma [6]. The presence of surface charges which is clearly necessary for a wall potential to develop is hard to reconcile with the instantaneous annihilation assumption. It is moreover almost always assumed that secondary electrons from the wall are released from the electronic bulk states and not from the electronic surface states which should in fact host the electrons accumulated from the plasma.

Following the lead of Emeleus and Coulter [7], [8] and others [9]–[11] who, respectively, introduced and applied the idea of a 2-D electron surface plasma attached to plasma walls, we recently proposed to visualize the charging of plasma walls as an electron physisorption process [12], [13]. In the surface-plasma-based physisorption scenario, the wall potential arises from 2-D electron and ion surface densities which, for a collisionless planar sheath, obey two coupled balance equations

$$\frac{dn_e}{dt} = s_e j_e^{\rm th} - \frac{n_e}{\tau_e} - \alpha_{\rm rw} n_i n_e \tag{1}$$

$$\frac{dn_i}{dt} = s_i j_i^{B} - \frac{n_i}{\tau_i} - \alpha_{\rm rw} n_i n_e \tag{2}$$

where $j_e^{\rm th}$ and j_i^B are, respectively, the thermal electron and the mono-energetic ion influx from the plasma. The surface properties are thereby encoded in the electron and ion sticking coefficients $s_{e,i}$, the electron and ion desorption times $\tau_{e,i}$, and the wall recombination constant $\alpha_{\rm rw}$. At quasi-stationarity, (1) and (2) reduce to

$$s_e j_e^{\rm th} = s_i j_i^B + \frac{n_e}{\tau_e} - \frac{n_i}{\tau_i} \tag{3}$$

which is a self-consistency equation for the wall potential ϕ_w, which enters through the thermal electron flux $j_e^{\rm th}$ and the electron surface density n_e. The perfect absorber approximation corresponds to $s_{e,i} = 1$ and $\tau_{e,i}^{-1} = 0$. To improve this approximation, one either has to measure $s_{e,i}$ and $\tau_{e,i}$ directly or calculate these quantities from microscopic models for the electron(ion)–wall interaction. Both is challenging. But advanced noninvasive techniques of measuring surface charges [14], [15] may successfully guide the construction of realistic microscopic models for the plasma wall.

We expect s_e and τ_e to be particularly important parameters, particularly in the early stages of the build-up of the wall potential. Using simple quantum-mechanical models for the electron–surface interaction, we calculated therefore these two quantities for uncharged metallic [13] and uncharged dielectric [16], [17] surfaces and found surprisingly small electron sticking coefficients. Only for metallic surfaces was the product $s_e\tau_e$ in the range expected from studies of dc column plasmas [9], [10] and grain charging [12].

Since we calculated s_e and τ_e only for uncharged surfaces, our previous results are only applicable to the very beginning of the charging process, when the wall is basically uncharged.

Manuscript received September 15, 2010; accepted October 12, 2010. Date of publication December 30, 2010; date of current version February 9, 2011.

The authors are with the Institute of Physics, Ernst-Moritz-Arndt-University Greifswald, 17489 Greifswald, Germany (e-mail: bronold@physik.uni-greifswald.de).

Digital Object Identifier 10.1109/TPS.2010.2094209

Below, we will extend our microscopic considerations to charged plasma walls. The electronic states on which the calculation of s_e and τ_e has to be based are then no longer the polarization-induced external surface states (image states) we employed for uncharged surfaces but unoccupied internal conduction band states of the wall. Nevertheless, the build-up of the wall potential can still be considered as an electron physisorption process.

In the next section, we qualitatively discuss general microscopic aspects of the electron–wall interaction. To be specific, we restrict ourselves to a planar dielectric wall. We then recall briefly in Section III the theoretical approach we employed previously to calculate s_e and τ_e for uncharged surfaces and present representative results for graphite and MgO. In Section IV, we describe a strategy to estimate s_e and τ_e for charged dielectric walls. Numerical results are given for a sapphire wall (Al_2O_3). We then combine our expressions for τ_e^{-1} and s_e with (3), setting $s_i = 1$ and $\tau_i^{-1} = 0$, to calculate the self-consistent wall potential beyond the perfect absorber model for electrons. It turns out to be roughly one-third of the perfect absorber value. Finally, Section V gives the conclusions we draw from our results.

II. Electron–Wall Interaction

To discuss the microscopic aspects of the electron–wall interaction, we consider a planar dielectric wall. It defines the xy-plane of a coordinate system separating the solid in the half-space $z \leq 0$ from the plasma in the half-space $z > 0$.

Quite generally, a quantum-mechanical calculation of the electron sticking coefficient s_e and electron desorption time τ_e has to be based on a Hamiltonian

$$H = H_e + H_w + H_{e-w} \tag{4}$$

where H_e, H_w, and H_{e-w} describe, respectively, the unperturbed dynamics of an electron in the vicinity of the wall, the elementary excitations of the wall responsible for electron energy relaxation, and the coupling between the two.

The electronic structure in the vicinity of the wall is rather complex. It depends on the plasma and the surface. Assuming, for simplicity, a perfect boundary, H_w is a single-electron Hamiltonian belonging to the electron potential energy

$$V(z) = \begin{cases} V_{\rm c}(z) & \text{for } z \leq 0 \\ V_{\rm p}(z) + V_{\rm s}(z) & \text{for } z > 0, \end{cases} \tag{5}$$

where $V_{\rm c}$ is the crystal potential of the wall material, $V_{\rm p}$ is the exchange- and correlation-induced polarization potential which confines the electrons inside the material and causes the attraction of external electrons to the surface at short distances, and $V_{\rm s}$ is the potential energy in the sheath which leads to a Coulomb barrier for electrons approaching the wall from the plasma. As explained in [13], $V(z)$ supports volume states (periodic inside the wall and exponentially decaying in the plasma), bound and unbound surface states (the former exponentially decaying on both sides of the plasma–wall interface and the latter decaying only inside the wall), as well as free states (nondecaying on both sides of the interface).

A plasma electron approaching the wall may get trapped (adsorbed) if it can get rid of its excess energy via inelastic scattering processes. Once it is trapped, it may de-trap again (desorb) if it gains enough energy from the wall. The scattering processes depend on the wall material. For dielectric walls, which have large energy gaps, optical and acoustic phonons cause energy relaxation whereas electron-hole pairs and plasmons trigger energy relaxation at metallic walls. The matrix elements of the coupling depend on whether surface or volume states are involved in the scattering process and thus on the microscopic details of the interface and the number of electrons already collected by the wall.

To determine what kind of electronic states are most likely involved in the build-up of the wall potential, it is instructive to consider the potential energy on the plasma side of the plasma–wall interface. For a collisionless sheath, it is given by

$$V(z > 0) = k_B T_e \eta_s(z) - \frac{1}{4}\frac{\epsilon_s - 1}{\epsilon_s + 1}\frac{e^2}{z} \tag{6}$$

where ϵ_s is the dielectric constant of the wall, e is the elementary charge, and $\eta_s(z)$ is the solution of [6]

$$\lambda_D^2 \frac{d^2\eta_s}{dz^2} = \frac{1}{\sqrt{1 + \frac{2\eta_s}{u_{i0}^2}}} - \exp[-\eta_s] \tag{7}$$

with $\lambda_D^2 = k_B T_e / e N_0$ the Debye screening length, $u_{i0} = v_i / \sqrt{k_B T_e / m_i}$ the ion velocity, and N_0 the volume plasma density; m_i is the ion mass and $k_B T_e$ is the mean electron energy in the plasma.

Fig. 1 shows $V(z > 0)$ for a MgO surface ($\epsilon_s = 9.8$) in contact with a He discharge whose mean electron energy $k_B T_e = 2$ eV and bulk plasma density is $N_0 = 10^{-7}$ cm^{-3}. To solve (7), we used the perfect absorber boundary condition; that is, we calculated the wall potential from $j_e^{\rm th} = j_i^B$ which leads to

$$-e\phi_w = \frac{1}{2} k_B T_e \ln\left[\frac{m_i}{2\pi m_e}\right]. \tag{8}$$

To mimic the build-up of the wall potential, we multiplied the perfect absorber value by the numerical factor attached to the graphs.

As can be seen close to the boundary, the potential energy decreases because of the polarization-induced attractive short-range part of the potential energy, the second term on the right-hand side of (6). Since MgO has a negative electron affinity $-\chi = 0.2$ eV $- 0.4$ eV [18], [19], the vacuum level is below the conduction band edge. Image states are thus possible and should control electron physisorption at the uncharged MgO surface. Once the surface is charged, the Coulomb barrier due to the sheath potential allows however only electrons with kinetic energy larger than the Coulomb repulsion to reach the wall. In that energy range, image states are unstable and the volume states indicated in the left panel of Fig. 1 are expected to be most important for adsorption to and desorption from the wall.

Having identified the physical processes leading, on the microscopic scale, to the build-up of a wall potential, we can now attempt a quantum-mechanical calculation of the electron

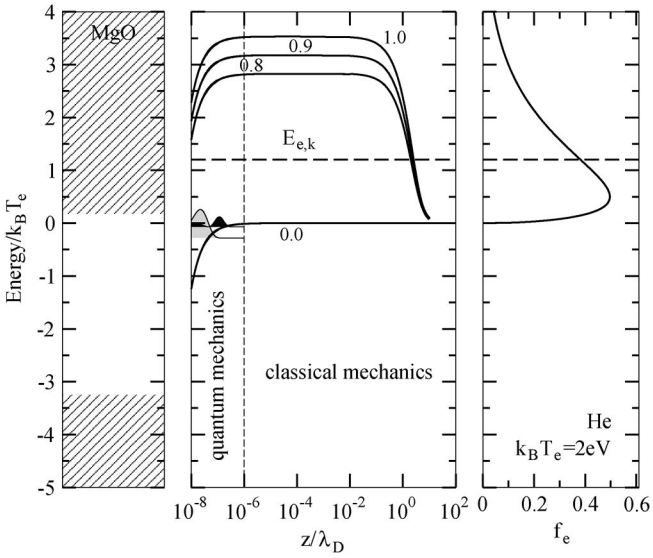

Fig. 1. Middle panel shows the potential energy of an electron in a collisionless sheath in front of a negatively charged dielectric boundary. Close to the boundary, the potential energy decreases because of the polarization-induced attraction. The number attached to the graphs give the wall potential in units of the perfect absorber value, (8). The material parameters are appropriate for a MgO wall, whose band structure is schematically shown in the left panel, and a He discharge with $N_0 = 10^7$ cm^{-3} and $k_B T_e = 2$ eV. The electron energy distribution function $f_e(E)$ in the bulk of the discharge is plotted on the right side of the panel. In the main panel are also shown the two lowest image states, controlling physisorption of an electron at an uncharged MgO surface. The processes close to or in the wall have to be described quantum-mechanically whereas the physics of the discharge is of course classical.

desorption time τ_e and the electron sticking coefficient s_e. This will be the topic of the next two sections.

III. Uncharged Dielectric Surfaces

If the electron affinity of an uncharged dielectric surface is negative, electron trapping and de-trapping occurs in polarization-induced external surface states (image states). In a theoretical approach patterned on that of physisorption of atoms and molecules [20], we calculated in [16], [17] s_e and τ_e for such a situation. For completeness, we recall in this section the main features of our approach and discuss representative data.

The starting point is a quantum-kinetic equation for the occupancies of the image states in [17, eq. (3)]

$$\begin{aligned}\frac{d}{dt}n_n(t) &= \sum_{n'}\left[\mathcal{W}_{nn'}n_{n'}(t) - \mathcal{W}_{n'n}n_n(t)\right] \\ &\quad - \sum_k \mathcal{W}_{kn}n_n(t) + \sum_k \tau_t \mathcal{W}_{nk}j_k \\ &= \sum_m T_{nm}n_m(t) + \sum_k \tau_t \mathcal{W}_{nk}j_k \end{aligned} \tag{9}$$

where $j_k \sim ke^{-\beta_e E_k}$ is the stationary flux corresponding to a single electron whose energy is distributed over the continuum of unbound surface states k with a mean electron energy $k_B T_e$, $\mathcal{W}_{q,q'}$ is the probability per unit time for a transition from state q' to q, which can be either bound $(q', q = n)$ or unbound $(q', q = k)$, arising from the interaction with a transverse acoustic phonon, which leads to an oscillation of the image plane, and $\tau_t = 2L/v_z$ is the traveling time through the surface potential of width L which, in the limit $L \to \infty$, can be absorbed into the transition probability per unit time from the continuum state k to the bound state n, $\mathcal{W}_{nk}$. In [16], we calculated the transition probabilities per unit time $\mathcal{W}_{q,q'}$ up to fourth order in the electron-phonon coupling for a recoil-corrected image potential which avoids the unphysical singularity of the classical image potential at $z = 0$.

The eigenvalues of the matrix $\mathbf{T}$ defined in (9) determine the time evolution of the occupancies $n_n(t)$. It turns out that $n_n(t)$ contains a quickly and a slowly varying part. Summing the slowly varying part, which we denoted by $n_n^s(t)$, over n, gives the overall probability $n^s(t)$ of the electron to remain in any of the bound surface states after the fast energy relaxation within the manifold of bound and unbound surface states deceased. The overall probability satisfies a first-order differential equation [17]

$$\frac{d}{dt}n^{\mathrm{s}}(t) = \sum_k s_{e,k}^{\mathrm{kinetic}} j_k - \frac{1}{\tau_e}n^{\mathrm{s}}(t) \tag{10}$$

with

$$s_{e,k}^{\mathrm{kinetic}} = \tau_t \sum_{n,l} e_n^{(0)} \tilde{e}_l^{(0)} \mathcal{W}_{lk} \tag{11}$$

the kinetic energy resolved sticking coefficient and

$$\tau_e^{-1} = \lambda_0 \tag{12}$$

the electron desorption time, where $e_n^{(0)}$ and $\tilde{e}_n^{(0)}$ are, respectively, the nth component of the right and left eigenvector corresponding to the lowest eigenvalue λ_0 of the matrix $\mathbf{T}$.

Equation (10) takes cascades between bound image states and re-emission after initial trapping into account. Initial trapping is the transition from a continuum state k to any bound state n. Its probability is given by the prompt energy resolved sticking coefficient

$$s_{e,k}^{\mathrm{prompt}} = \tau_t \sum_n \mathcal{W}_{nk}. \tag{13}$$

For the situation we consider, a stationary incident unit electron flux corresponding to an electron with Boltzmann distributed kinetic energies, it is more appropriate to discuss energy averaged sticking coefficients

$$s_e^{\cdots} = \frac{\sum_k s_{e,k}^{\cdots} k e^{-\beta_e E_k}}{\sum_k k e^{-\beta_e E_k}} \tag{14}$$

where $\beta_e^{-1} = k_B T_e$ is the mean electron energy.

Using the approach just outlined, we investigated in great detail trapping [17] and de-trapping [16] of an electron to-and-fro an uncharged dielectric surface. Of particular importance is thereby the depth of the surface potential which we classified as one-, two-, and multiphonon deep depending on whether the transition between the lowest two bound surface states requires one-, two-, or multiphonons. Beyond the two-phonon processes, the calculation of the transition probabilities is very tedious. We restricted ourselves therefore to one- and two-phonon deep potentials as it is applicable, for instance, to

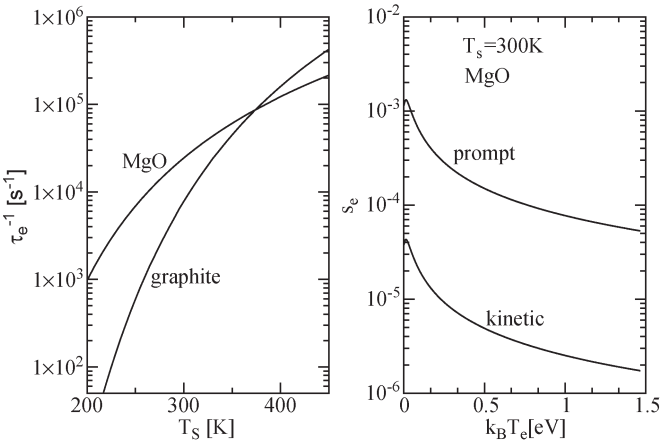

Fig. 2. Inverse electron desorption time for an electron thermalized in the bound surface states of a MgO and a graphite surface (left panel) and prompt and kinetic electron sticking coefficient (right panel) for an electron whose kinetic energy is Boltzmann distributed over the unbound surface states of a MgO surface.

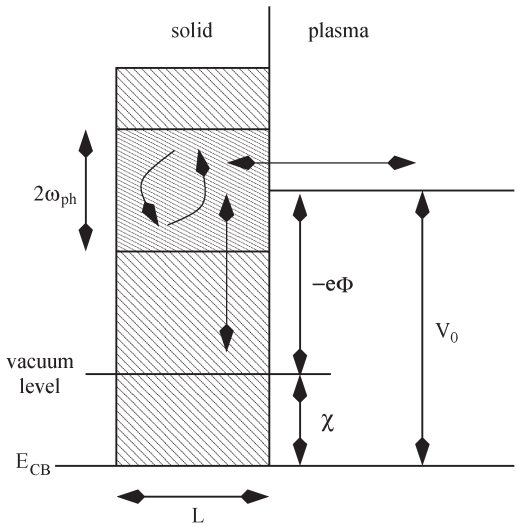

Fig. 3. Illustration of the model used to estimate the electron desorption time and electron sticking coefficient for a charged dielectric surface.

graphite and MgO. Sapphire (Al_2O_3), the dielectric we will consider in the next section, has a three-phonon deep surface potential.

In Fig. 2, we plot representative results for graphite and MgO. The electron desorption times vary strongly with the surface temperature T_s. The temperature dependence is exponential and can be fitted by an Arrhenius-like expression $\tau_e^{-1} = cT_s e^{-E_d/k_B T_s}$ with c and E_d as fit parameters. The parameter E_d can be interpreted as the desorption energy but it does not coincide with the binding energy of the lowest bound surface state as one might expect. The pre-exponential factor cT_s is also not the frequency at the bottom of a potential well as it is sometimes erroneously assumed. The electron sticking coefficients shown in the right panel of Fig. 2 are rather small, in particular, the kinetic sticking coefficients, which are always smaller than the prompt sticking coefficients because they account for the possibility that the electron may de-trap after initial trapping.

Empirical fits to s_e and τ_e obtained from applications of the surface plasma model to dc column plasmas [9], [10] suggest $s_e\tau_e \approx 10^{-6}$ s whereas our microscopic calculation for an uncharged dielectric surface leads to $s_e\tau_e \approx 10^{-8}$ s or even smaller depending on the electron temperature. The reason for the discrepancy is the neglect of the wall potential. The approach discussed in this section is only applicable to an uncharged dielectric surface, where the vacuum potential is below the conduction band edge. As we have seen in the previous section, for a charged plasma wall, electrons already trapped on or in the wall lead to a Coulomb barrier for the approaching electron. Charge collection takes then place in an energy region where empty conduction band states are available. In the next section, we shall discuss the dramatic change in the physisorption microphysics which originates from this fact.

IV. Charged Dielectric Walls

Plasma walls carry a negative potential of typically a few electron volts. Only electrons with a kinetic energy large enough to overcome the Coulomb barrier due to this potential have a chance to come close enough to the surface to experience the polarization-induced attraction. In this energy range, however, polarization-induced image states are unstable because of the existence of empty conduction band states. In our notation, trapping and de-trapping of an electron no longer involves transitions between bound and unbound surface states but transitions between free states and volume states. The "surface charge," is thus not localized in front of the wall but occupies part of the interior of the wall.

The build-up of the wall potential can be still understood as an electron physisorption process involving now, however, free states and the continuum of volume states in the conduction band and not the continuous and discrete spectrum of unbound and bound surface states. Instead of a dynamic perturbation of the surface potential, triggered by an acoustic phonon leading to an oscillation of the image plane, electron energy relaxation is now due to inelastic scattering processes within the wall, involving acoustic and optical bulk phonons and, if the electron energy is larger than the energy gap of the dielectric, impact ionization of valence electrons. Elastic scattering on impurities may also contribute to temporary charge trapping.

In the following, we give a rough estimate of the electron desorption time and the electron sticking coefficient for a charged dielectric wall. A more accurate calculation, taking a realistic electronic structure of the wall and all relevant scattering processes into account, will be presented elsewhere [21].

The model on which our estimate is based is shown in Fig. 3. Motivated by Fig. 1, we approximate the potential energy in the vicinity of the wall by a potential step of height $V_0 = -e\phi + \chi$, where χ is the electron affinity of the wall and $-e\phi$ is the potential energy at the wall [the self-consistent wall potential (see below) we call ϕ_w]. Neglecting multiphonon processes, the energy interval $[V_0 - \hbar\omega_{\rm ph}, V_0 + \hbar\omega_{\rm ph}]$ with $\hbar\omega_{\rm ph}$ the energy of an optical phonon is essential for trapping and de-trapping of an electron.

Using the notation introduced in [13] and briefly mentioned in the previous section, an electron in a free state with energy between $V_0 + \hbar\omega_{\rm ph}$ and V_0 has a chance to end up via one-phonon emission in a volume state below V_0 (see Fig. 3). Since the thermalization in the conduction band of an insulator is extremely fast, occurring on the fs time scale [22], once the electron is in a state below V_0, it quickly relaxes to the lowest available volume state, which, leaving defect states aside, will be close to the bottom of the conduction band. Desorption from such a deep state, the "electron binding energy" is of the order of V_0, is quite unlikely. Within the one-phonon approximation, desorption can only occur if the trapped electron has an energy between $V_0 - \hbar\omega_{\rm ph}$ and V_0 and absorbs a phonon. The probability for occupying such high-lying volume states at room temperature is extremely small. Even without calculation, we can already note that a charged wall will have a much longer electron desorption time than an uncharged one.

To complete the mathematical formulation of the model, we need a length scale L on which energy relaxation takes place. For the uncharged wall, this was the range of the surface potential. Since for a charged wall energy relaxation takes place inside the wall, this length is no longer applicable. Instead, it is the penetration depth of the electron which now determines the efficiency with which it loses energy and gets pushed into bound states below V_0. In principle, the penetration depth can be calculated from a Boltzmann equation, taking all relevant scattering processes into account but it is quite expensive. For the purpose of this paper, which is to discuss possible microscopic scenarios, we postpone such a calculation. Using the penetration depth as an adjustable parameter taken from experiments, we can nevertheless produce reasonable first estimates for s_e and τ_e.

Ignoring cascades within the continua of free and volume states, respectively, the electron desorption time and the electron sticking coefficient can be obtained from second-order perturbation theory with respect to the bulk electron-phonon coupling. More specifically,

$$\tau_e^{-1} = \langle \Gamma_{\vec{Q}q} \rangle_D \text{ and } s_e = \langle S_{\vec{K}k} \rangle_P \tag{15}$$

with

$$\Gamma_{\vec{Q}q} = \sum_{\vec{K}k} \mathcal{W}^-(\vec{K}k, \vec{Q}q) \tag{16}$$

$$S_{\vec{K}k} = \frac{2Lm^*}{\hbar k} \sum_{\vec{Q}q} \mathcal{W}^+(\vec{Q}q, \vec{K}k) \tag{17}$$

$$\mathcal{W}^{\pm}(\vec{k}, \vec{k}') = \frac{2\pi}{\hbar} \left| M(|\vec{k} - \vec{k}'|) \right|^2 \delta(E_{\vec{k}'} - E_{\vec{k}} \mp \hbar\omega_{\rm ph}) \times \left[n_B(\hbar\omega_{\rm ph}) + \frac{1}{2} \pm \frac{1}{2} \right] \tag{18}$$

where

$$n_B(\hbar\omega_{\rm ph}) = \frac{1}{\exp(\hbar\omega_{\rm ph}/k_B T_l) - 1} \tag{19}$$

with T_l the lattice temperature of the wall. The function

$$M\left(|\vec{k} - \vec{k}'|\right) = -2i\sqrt{\frac{\hbar\omega_{\rm ph}(\epsilon_\infty^{-1} - \epsilon_s^{-1})}{2Ve^2}} \frac{e^2}{|\vec{k} - \vec{k}'|} \tag{20}$$

is the matrix element for the scattering of a conduction band electron off a polar phonon for vanishing conduction band electron density [23]; V is the volume occupied by the wall and ϵ_∞ and ϵ_s are, respectively, the high frequency and the static limit of the dielectric function of the wall.

The energy of a bound electron, that is, an electron in a volume state, is $E_{\vec{Q}q} = \hbar^2 Q^2/2m^* + E_q$ with $E_q = \hbar^2 q^2/2m^* < V_0$, where m^* is the effective electron mass of the conduction band, and $\vec{Q}$ and q are, respectively, the 2-D momentum lateral and normal to the wall. For an unbound electron, that is, an electron in a free state, the energy is $E_{\vec{K}k} = \hbar^2 K^2/2m^* + E_k$ with $E_k = \hbar^2 k^2/2m^* > V_0$ and $\vec{K}$ and k having the same meaning for an unbound electron as $\vec{Q}$ and q for a bound one. If the unbound electron is in the plasma half-space, the effective mass has to be replaced by the bare electron mass m_e.

The brackets in (16) and (17) indicate averages with respect to the weight functions D and P, respectively. The former can be interpreted as the probability for a trapped electron to have the energy $E_{\vec{Q}q}$. It is given by

$$D_{\vec{Q}q} = \frac{\exp[-\beta_{\rm eff} E_{\vec{Q}q}]}{\sum_{\vec{Q}'q'} \exp[-\beta_{\rm eff} E_{\vec{Q}'q'}]} \tag{21}$$

with an effective electron temperature $T_{\rm eff} = 1/k_B\beta_{\rm eff}$. Since we expect electrons in the conduction band of the wall to be thermalized, the effective temperature is equal to the lattice temperature which in turn is of the order of the room temperature and thus very low compared to the electron temperature T_e and the potential height V_0. The weight function used in the definition of the sticking coefficient is

$$P_{\vec{K}k} = \frac{\exp[-\beta_e E_{\vec{K}k}]k}{\sum_{\vec{K}'k'} \exp[-\beta_e E_{\vec{K}'k'}]k'}. \tag{22}$$

In the narrow energy range around V_0 where trapping and detrapping occurs (see Fig. 3) the momentum dependence of $\Gamma_{\vec{Q}q}$ and $S_{\vec{K}k}$ is weak. We calculate therefore both quantities only for vanishing lateral momentum (implying normal incident) and normal momentum equal to $(2m^*V_0/\hbar^2)^{1/2}$. Utilizing moreover that $\hbar\omega_{\rm ph} \ll V_0$, the integrals defining τ_e and s_e can be done analytically.

Measuring energies in units of the Rydberg energy Ry and lengths in units of the Bohr radius a_B and introducing a dimensionless electron-phonon coupling constant

$$C = 4\omega_{\rm ph}\left(\frac{1}{\epsilon_\infty} - \frac{1}{\epsilon_s}\right) \tag{23}$$

we find for the inverse electron desorption time

$$\tau_e^{-1} = \sqrt{\frac{m^*}{m_e}\frac{\beta_{\rm eff}\omega_{\rm ph}^2}{\pi V_0^2}} \frac{C}{8\pi} \ln\left[\frac{4V_0}{\omega_{\rm ph}}\right] \exp\left[-\beta_{\rm eff} V_0\right] \frac{Ry}{\hbar} \tag{24}$$

and for the prompt electron sticking coefficient

$$s_e = \frac{m^*}{m_e}\frac{\beta_e\omega_{\rm ph}}{V_0}\frac{C}{8\pi}\ln\left[8\left(\frac{V_0}{\omega_{\rm ph}}\right)^2\right]\exp[-\beta_e\omega_{\rm ph}]\frac{L}{a_B}d. \quad (25)$$

Since we do not allow for the possibility that an initially trapped electron may desorb before it relaxes to the deep conduction band states, we cannot distinguish between prompt and kinetic sticking.

In order to see what electron desorption times and electron sticking coefficients can be expected for a charged wall, we present data for a charged sapphire surface (Al_2O_3). The material parameters for sapphire are well known because of its importance for microelectronics. In sapphire, there are two optical phonon modes which couple strongly to electrons: 1) a longitudinal; and 2) a transverse one. The energy of both modes is approximately $\hbar\omega_{\rm ph} = 0.1$ eV [24] and the dielectric constants determining the coupling strength for both modes are approximately $\epsilon_\infty = 3$ and $\epsilon_s = 9$ [25]. To account for the two modes, we can thus simply multiply the transition rates by a factor of two and use the given parameter set. The effective mass of conduction band electrons in sapphire is $m^* = 0.3m_e$ [24]. As far as the penetration depth of electrons is concerned, we first note that after overcoming the Coulomb barrier, the electrons in question have a kinetic energy of only a few electron volts. Measurements on Al_2O_3 tunneling diodes have shown that in this energy range, electrons have penetration depths between 50 and 200 Å [26], [27].

First, we discuss the electron desorption time τ_e. As already mentioned, electrons in the conduction band of an insulator thermalize with the lattice on a fs time scale [22]. The mean energy of a trapped electron is thus $k_BT_{\rm eff} = k_BT_l \approx 0.026$ eV. Since, on the other hand, $V_0 = -e\phi + \chi$ is typically a few electron volts, the exponential factor in (24) is extremely small, implying $\tau_e^{-1} \approx 0$ as assumed in the perfect absorber model. In the initial stages of charge accumulation, however, when the wall potential is not yet fully developed, desorption cannot be neglected.

Let us now turn to the electron sticking coefficient. Fig. 4 shows for various penetration depths the electron sticking coefficient as a function of the wall potential. For our model to be applicable, the Coulomb barrier of the wall has to be larger than the phonon energy. Hence, the data shown in Fig. 4 apply only to situations where $-e\phi + \chi > \hbar\omega_{\rm ph} \approx 0.1$ eV. Compared to the sticking coefficients of an uncharged dielectric surface with negative electron affinity, the sticking coefficients are three orders of magnitude larger. Because energy relaxation takes now place inside the wall an initially unbound electron couples strongly to bulk phonon modes. It can thus lose energy very efficiently, leading to electron sticking coefficients of the order of 10^{-1} and not of the order of 10^{-4}. Note, however, in reality, the sticking coefficient might be somewhat smaller because we neglected re-emission of the electron before thermalization in the conduction band is completed and implicitly assumed that the transmission probability of a plasma electron to the solid is one, whereas in reality, it is energy-dependent and always less than one because of the difference in the mass.

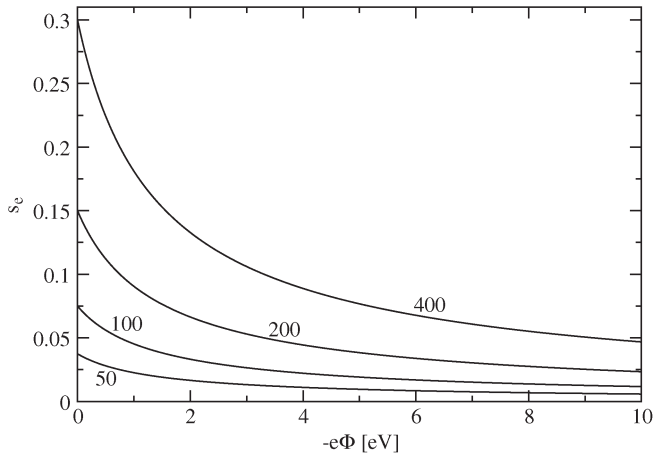

Fig. 4. Prompt electron sticking coefficient for a sapphire surface (Al_2O_3) at room temperature as a function of the wall potential ϕ and the electron penetration length L. The numbers attached to each graph indicate L in units of the Bohr radius a_B. Note, the applicability of the model on which the calculation of s_e is based requires $-e\phi + \chi > \hbar\omega_{\rm ph} \approx 0.1$ eV.

Equations (24) and (25) give, respectively, the electron desorption time and electron sticking coefficient as a function of V_0 and hence of ϕ. We can thus use these two equations to determine the self-consistent wall potential ϕ_w for a collisionless sheath, taking surface effects beyond the perfect absorber approximation for electrons into account. Setting $s_i = 1, \tau_i^{-1} = \tau_e^{-1} = 0$, and inserting (25) into (3) gives a transcendental equation for $-e\phi$, whose root is $-e\phi_w$. Recall, we considered only scattering on two optical phonon modes. In reality, there is also scattering on acoustic phonons as well as impurities which can also push electrons into states which are temporarily bound with respect to their normal motion. The wall potential we obtain is thus a lower bound to the true wall potential, whereas the wall potential of the perfect absorber is certainly an upper bound.

As can be seen in the lower panel of Fig. 5, the wall potential including surface effects for electrons is roughly one-third of the wall potential of the perfect absorber, (8). The true wall potential should be somewhere between our result and the perfect absorber value. The accuracy of our theoretical estimate is of course not good enough to make more precise statements. The same may be unfortunately said about experimental measurements. Nevertheless, it is encouraging that the approximate expressions (24) and (25) produce in conjunction with (3) wall potentials of the expected order of magnitude. The upper panel of Fig. 5 finally shows that the electron sticking coefficient of a charged wall is of the order of 10^{-1} and thus significantly smaller than assumed in the perfect absorber model.

V. Conclusion

The purpose of this paper was to discuss the interaction of plasma electrons with plasma walls beyond the perfect absorber approximation. Instead of assuming an electron hitting the wall to be absorbed with certainty and never released again, we proposed a physisorption-inspired quantum-mechanical model to calculate the probability with which an electron gets stuck to the plasma wall—the electron sticking coefficient s_e—and

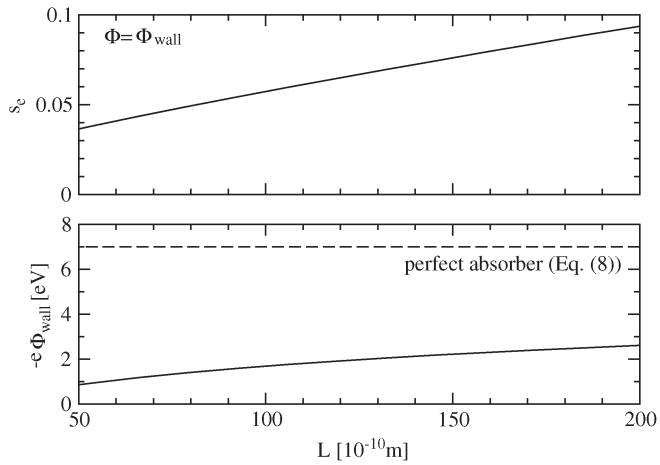

Fig. 5. (Lower panel) Self-consistent wall potential ϕ_w for a sapphire surface in contact with a helium discharge as a function of the electron penetration length L. (Upper panel) Prompt electron sticking coefficient at the selfconsistent wall potential. The mean electron energy in the discharge is $k_B T_e = 2$ eV.

the time the electron remains on or in the wall—the electron desorption time τ_e.

The microphysics controlling s_e and τ_e depends on the charge of the wall. When the wall is uncharged, that is, in the early stages of the charging process and has a negative electron affinity sticking and desorption occurs in polarization-induced external-bound surface states (image states) and is triggered by inelastic scattering cascades with acoustic phonons. The sticking coefficient s_e is then very small, at most of the order of 10^{-4}, and the desorption time $\tau_e \approx 10^{-4}$ s. The wall is thus far from being a perfect absorber for electrons which would correspond to $s_e = 1$ and $\tau_e^{-1} = 0$.

Once the wall is charged, the negative wall potential ϕ blocks surface and volume states between the vacuum level and the Coulomb barrier. An approaching electron overcoming the Coulomb barrier may then directly enter empty conduction band states, that is, volume states which do not exponentially decay inside the bulk of the wall as image states do. Electron energy relaxation due to inelastic scattering with optical bulk phonons may then be very efficient in pushing the electron below the Coulomb barrier. As a result, it gets stuck. Once it is stuck, thermalization with the lattice is very fast, implying that the stuck electron relaxes quickly to the bottom of the conduction band from which it cannot escape at room temperature. Within this scenario, the binding energy of the trapped electrons is approximately $-e\phi + \chi$, where ϕ is the actual wall potential and χ is the electron affinity of the wall, s_e is of the order of 10^{-1} and $\tau_e^{-1} \approx 0$. Hence, if it was not for s_e, the wall would be a perfect absorber.

Calculating s_e and τ_e as a function of the wall potential ϕ and inserting these two expressions in the quasi-stationary balance equations for the electron and ion surface densities of a collisionless sheath while assuming the wall to be a perfect absorber for ions, we obtained the self-consistent wall potential ϕ_w beyond the perfect absorber approximation for electrons. Taking electron surface effects into account reduces ϕ_w approximately by a factor of three compared to the perfect absorber value.

Our investigation clarifies the materials science aspects which have to be resolved in order to go beyond the perfect absorber model for electrons. The most important one is of course the precise electronic structure of the wall, including defect states due to surface reconstruction and/or chemical contamination because it determines the nature of the states which potentially host the electrons building up the wall potential. But also the thermalization and penetration of electrons with only a few electron volts of kinetic energy are critical processes. From low-energy electron diffraction, it is known that in this energy range, the interaction of electrons with solids is particularly intricate. Although the accuracy of the perfect absorber model for electrons might be sufficient for the modeling of traditional electrical discharges, for the modeling of dusty plasmas, and solid-state-based microdischarges. the description of the electron–wall interaction along the lines presented here will be vital.

ACKNOWLEDGMENT

Support from the Deutsche Forschungsgemeinschaft through the Transregional Collaborative Research Center 24 is greatly acknowledged. J. Marbach is supported by the International Max Planck Research School for Bounded Plasmas.

REFERENCES

[1] O. Ishihara, "Complex plasma: Dusts in plasma," *J. Phys. D, Appl. Phys.*, vol. 40, no. 8, pp. R121–R147, Apr. 2007.
[2] V. E. Fortov, A. V. Ivlev, S. A. Khrapak, A. G. Khrapak, and G. E. Morfill, "Complex (dusty) plasmas: Current status, open issues, perspectives," *Phys. Rep.*, vol. 421, no. 1/2, pp. 1–103, Dec. 2005.
[3] D. A. Mendis, "Progress in the study of dusty plasmas," *Plasma Sources Sci. Technol.*, vol. 11, no. 3A, pp. A219–A228, Aug. 2002.
[4] M. J. Kushner, "Modelling of microdischarge devices: Plasma and gas dynamics," *J. Phys. D, Appl. Phys.*, vol. 38, no. 11, pp. 1633–1643, Jun. 2005.
[5] K. H. Becker, K. H. Schoenbach, and J. G. Eden, "Microplasmas and applications," *J. Phys. D, Appl. Phys.*, vol. 39, no. 3, pp. R55–R70, Feb. 2006.
[6] R. N. Franklin, *Plasma Phenomena in Gas Discharges*. Oxford, U.K.: Clarendon, 1976.
[7] K. G. Emeleus and J. R. M. Coulter, "Kinetic theory of the surface recombination of electrons and ions on glass surfaces," *Int. J. Electron.*, vol. 62, no. 2, pp. 225–227, 1987.
[8] K. G. Emeleus and J. R. M. Coulter, "Surface recombination of ions and cratering by ion impact," *Proc. Inst. Elect. Eng.*, vol. 135, no. 1, pp. 76–78, Jan. 1988.
[9] J. F. Behnke, T. Bindemann, H. Deutsch, and K. Becker, "Wall recombination in glow discharges," *Contrib. Plasma Phys.*, vol. 37, no. 4, pp. 345–362, 1997.
[10] D. Uhrlandt, M. Schmidt, J. F. Behnke, and T. Bindemann, "Self-consistent description of the dc column plasma including wall interaction," *J. Phys. D, Appl. Phys.*, vol. 33, no. 19, pp. 2475–2482, Oct. 2000.
[11] Y. B. Golubovskii, V. A. Maiorov, J. Behnke, and J. F. Behnke, "Influence of interaction between charged particles and dielectric surface over a homogeneous barrier discharge in nitrogen," *J. Phys. D, Appl. Phys.*, vol. 35, no. 8, pp. 751–761, Apr. 2002.
[12] F. X. Bronold, H. Fehske, H. Kersten, and H. Deutsch, "Surface states and the charge of a dust particle in a plasma," *Phys. Rev. Lett.*, vol. 101, no. 17, p. 175 002, Oct. 2008.
[13] F. X. Bronold, H. Deutsch, and H. Fehske, "Physisorption kinetics of electrons at plasma boundaries," *Eur. Phys. J. D*, vol. 54, no. 3, pp. 519–544, Sep. 2009.
[14] A. Kumada, T. Sugihara, M. Chiba, and K. Hidaka, "Two-dimensional potential distribution measurement of surface charge with subnanosecond resolution," *Rev. Sci. Instrum.*, vol. 73, no. 4, pp. 1939–1944, Apr. 2002.
[15] L. Stollenwerk, J. G. Laven, and H.-G. Purwins, "Spatially resolved surface-charge measurement in a planar dielectric-barrier discharge system," *Phys. Rev. Lett.*, vol. 98, no. 25, p. 255 001, Jun. 2007.

[16] R. L. Heinisch, F. X. Bronold, and H. Fehske, "Phonon-mediated desorption of image-bound electrons from dielectric surfaces," *Phys. Rev. B, Condens. Matter*, vol. 81, no. 15, p. 155 420, Apr. 2010.
[17] R. L. Heinisch, F. X. Bronold, and H. Fehske, "Phonon-mediated sticking of electrons at dielectric surfaces," *Phys. Rev. B, Condens. Matter*, vol. 82, no. 12, p. 125 408, Sep. 2010.
[18] B. Baumeier, P. Krüger, and J. Pollmann, "Bulk and surface electronic structures of alkaline-earth metal oxides: Bound surface and image-potential states from first principles," *Phys. Rev. B, Condens. Matter*, vol. 76, no. 20, p. 205 404, Nov. 2007.
[19] M. Rohlfing, N.-P. Wang, P. Krüger, and J. Pollmann, "Image states and excitons at insulator surfaces with negative electron affinity," *Phys. Rev. Lett.*, vol. 91, no. 25, p. 256 802, Dec. 2003.
[20] H. J. Kreuzer and Z. W. Gortel, *Physisorption Kinetics*. Berlin, Germany: Springer-Verlag, 1986.
[21] R. L. Heinisch, F. X. Bronold, H. Fehske, unpublished.
[22] H.-J. Fitting, "Ultrafast relaxation of electrons and selfconsistent electrical charging in insulators," *Radiat. Meas.*, vol. 45, no. 3–6, pp. 530–532, Mar.–Jul. 2010.
[23] B. K. Ridley, *Quantum Processes in Semiconductors*. Oxford, U.K.: Clarendon, 1999.
[24] J. Shan, F. Wang, E. Knoesel, M. Bonn, and T. F. Heinz, "Measurement of the frequency-dependent conductivity of sapphire," *Phys. Rev. Lett.*, vol. 90, no. 24, p. 247 401, Jun. 2003.
[25] M. Schubert, T. E. Tiwald, and C. M. Herzinger, "Infrared dielectric anisotropy and phonon modes of sapphire," *Phys. Rev. B, Condens. Matter*, vol. 61, no. 12, pp. 8187–8201, Mar. 2000.
[26] W. Pong, "Photoemission from Al-Al_2O_3 films in the vacuum ultraviolet region," *J. Appl. Phys.*, vol. 40, no. 4, pp. 1733–1739, Mar. 1969.
[27] T. W. Hickmott, "Electron emission, electroluminescence, and voltage-controlled negative resistance in Al-Al_2O_3-Au diodes," *J. Appl. Phys.*, vol. 36, no. 6, pp. 1885–1896, Jun. 1965.

Author photographs and biographies not available at the time of publication.